



Cite this: *Mater. Adv.*, 2025, 6, 6585

Flame-retardant impregnation of flexible hybrid-silica marshmallow aerogels for lightweight transportation

Danny Bialuschewski, ^a Kai Steffens ^a and Barbara Milow ^{ab}

One of the main drawbacks for hybrid-silica aerogels is their flammability, an inherent property of the organic groups which severely limits their potential. This research is an important step to produce viable aerogels and take advantage of their low thermal conductivity and very low density, for example as lightweight insulation material used in aircraft cabins or other vehicles. Within this work, three different flexible hybrid-silica aerogel systems with different shapes and densities were investigated towards their burn behavior before and after soaking with the flame-retardant triphenyl phosphate (TPP). For this, different concentrations and evaporation temperatures were used before ultimately burning the samples while tracking the duration of the different fire stages. This data was used to calculate their flammability and overall performance for lightweight application in airplanes. In addition to this, other pre- and post-burn analysis like IR, TGA or melting behavior were performed. In the end, we were able to produce promising samples with good flame-retardancy at only minimal increase in density, an overall key combination useful for many different applications.

Received 30th June 2025,
Accepted 12th August 2025

DOI: 10.1039/d5ma00695c

rsc.li/materials-advances

Introduction

Aerogels are highly porous low-weight materials with a very high surface area and remarkable thermal insulation properties.^{1,2} The most well-researched, classic silica aerogels, are also non-flammable with a melting point of 1400 °C and operating temperature of -273 °C to 650 °C.³ The most common application is in the field of thermal insulation,⁴ for example in transportation as fibers⁵ or in construction as high performance aerogel concrete (HPAC), a mixture of silica aerogel granules embedded in a cement matrix.⁶

However, these aerogels are very rigid and hydrophilic by nature, limiting their applicability. Both challenges can be tackled by introducing organic groups to the system, leading to flexible and hydrophobic hybrid-silica aerogels, which can also be dried at ambient pressure instead of supercritical conditions, saving time and more costly solvent exchange.^{7,8} These hybrid materials, often called marshmallows due to their white color and softness, offer a vastly wider range of uses especially as composites.⁹ For example, double-crosslinked silica-hybrids could be superinsulators, adsorbents, sensors and much more.¹⁰ Yet these hydrocarbon chains oxidize

around 200 °C, limiting the material where thermal stability is important.¹¹ There are several methods to counteract this, for example by introducing flame-retardant compounds, something already used in the field of polymer production.¹²

Low weight, flame-retardancy, hydrophobicity and flexibility are all important factors in the transportation industry, where aerogel mats are already investigated as aircraft cabin insulation.¹³ The state-of-the-art are fibers made of glass in thin polymeric packaging.¹⁴ While these have high protection against fire, their hydrophilic nature easily leads to accumulated moisture, which can lead to higher corrosion of the aluminum airframe or molding.¹⁵ Currently the only prevention is decreasing the humidity level, which in turn lowers the comfort of the passengers.¹⁶ Fire resistance is especially important in aircrafts: a two-minute delay of smoke and fire spreading in-flight could be the difference between successful landing with evacuation or complete loss of both the aircraft and everyone inside according to the Federal Aviation Administration (FAA).¹⁷

There are two dominant mechanisms for the flame-retarding effect: the formation of a protective char-layer in the solid phase, shielding the material from oxygen, in turn suffocating the flame and preventing further formation of reactive gasses while also reducing the smoke that escapes;¹⁸ the other prevents further burning in the gas phase, for example by scavenging the reactive hydrogen and hydroxyl radicals¹⁹ with certain compound released under heat. These can include non-flammable gases

^a Nanostructured Cellular Materials, University of Cologne, Greinstr. 6, 50939 Cologne, Germany. E-mail: Danny.Bialuschewski@uni-koeln.de
Institute for Frontier Materials on Earth and in Space, German Aerospace Center, Linder Höhe, 51147 Cologne, Germany



that dilute oxygen. This slows down the burning process and in turn limits the fire from spreading.²⁰

There are several different types with their own advantages and disadvantages. Metal-based flame-retardance, like aluminum tri-hydrate (ATH) in addition to the protective layer, can release H₂O as non-flammable gas during combustion.²¹ Yet they have a higher density (2.42 g cm⁻³ for ATH)²² than their metal-free alternatives, making them unsuitable for lightweight applications. For halogenated species, in addition to the char-layer, the halogenated part reacts in the gas phase.²³ While this leads to a protected material, it also produces toxic compounds, resulting in more and more regulations prohibiting their use.^{24,25} Phosphorus flame-retardant, specifically non-halogenated organophosphates,²⁵ will lead to a polymeric type of phosphonic acid under heat, resulting in the char layer.¹⁸ Its' influence on the gas phase reaction depends highly on the organophosphate used, and can range from nearly none to an effect similar to halogenated species.²⁶ They usually have low density in comparison to the metal-based alternatives (~1 to 1.3 vs. ~2.4 g cm⁻³),²⁷ making them a potential candidate in see desired applications.

There are several examples in literature focused on a singular part of this topic. Hybrid-silica aerogels had improved flame-retardancy by growing a polyimide chain *in situ* by SCLD (stepwise chemical liquid deposition).²⁸ Organophosphate flame-retardants have also been investigated with aerogels, for example polyvinyl phosphate in cellulose aerogels²⁹ or vinyl phosphonic acid on textiles.³⁰ Additionally, they were investigated as additive for potential aircraft furnishing or fiber composite structures,³¹ for example as finish on cotton fibers³² or polyesters and nylons.³³ However, combining the topics of alkylated silica aerogels and organophosphate as flame-retardant tailored towards lightweight transportation, for example aircrafts, has to our knowledge not yet been published.

Experimental

Experiments and synthesis

The full aerogel synthesis consists of several steps: preparation of the sol, gelation, aging, washing and shrinkage-free drying. All chemicals were used as received.

In order to obtain a standard aerogel monolith, a batch of 100 ml sol is prepared according to our patent³⁴ by dissolving 20 g (33 mmol, 3.97 eq.) urea in 48 ml (3.34 mol, 39.65 eq.) of DI-water under stirring at 50 °C. After that, 19 µl (0.34 mmol, 0.004 eq.) of glacial acetic acid is added, and everything stirred for five minutes at 50 °C. Then, 12 ml (84 mmol, 1 eq.) of methyltrimethoxysilane (MTMS) and 16.7 ml (13 mmol, 0.15 eq.) of the surfactant hexadecyltrimethylammonium chloride (CTAC) was added and the solution further stirred for 15 minutes at 50 °C. Afterwards, 7.7 ml (56 mmol, 0.67 eq.) of dimethyldimethoxysilane (DMDMS) was added and the mixture stirred for another 45 minutes at 50 °C to produce the final sol. For gelation and aging, around 25 ml of the sol was filled in 60 ml screwcap polypropylene container, which was tightened and placed into an oven at 80 °C for 24 hours. Washing of the samples took place

after demolding and involved two water, one ethanol and a final water step with each lasting 24 hours. Roughly two-times the sample volume was used as amount of washing solvent. For drying, the wet samples were placed freely in an oven at 80 °C for 24 hours. The complete drying was verified by checking for a constant mass.

To prepare sol for a diluted aerogels monolith batch, the synthesis remains identical except the use of 86.4 ml (5.47 mol, 65 eq.) of DI water in total, leading to 138 ml of sol, and the aging time extended to seven days.

In order to produce aerogel pellets, the recipe remains identical to the standard aerogel monolith, but instead of filling the sol in screwcap-containers, it is filled into many half-sphere-shaped molds ($d = 1.2$ cm) made of silicone and put into a closed container for the gelation and aging step. They were demolded after aging.

To introduce the flame retardant into the dried aerogel samples, triphenyl phosphate (TPP) was dissolved in ethanol (tech. grade) to obtain different concentrations (5 to 150 g l⁻¹). The samples were soaked in 20 ml of this solution for 2 hours. The solvent was then evaporated at different temperatures (room temperature to 80 °C) until dried, verified by checking for constant mass. Before further calculations and experiments, any loosely grown TPP crystals were softly removed with cleaning paper.

Flammability experiments were performed where the monolithic sample or 15 pellets were placed on top of a metal grid and clamped, with a distance to the torch head of 10 cm. The flame was directed at the sample for either 20 or 40 second directly from below. The whole burn process was filmed and evaluated afterwards.

To investigate the melting behavior of the flame-retardant inside the aerogel, the infiltrated samples were placed on a 100 °C heating plate inside weighted beakers for up to six hours. The temperature of the plate (internal temperature probe), the top and inside the sample (both with external temperature sensors) was tracked and also verified by an IR temperature sensor.

Equipment

The stirring and heating plates used were MR Hei-Standard with the temperature control from EKT-Hei-Con, both from Heidolph.

For temperature verification a digital infrared thermometer HT3300 from HT Instruments was used.

For drying, the ovens used were either UE200 or UF1060plus, both from Memmert.

The burn experiments were performed using a gas cartridge multigas® 300, consisting of 30% Propane and 70% Butane, from ROTHENBERGER Industrial, with the burn process being filmed with an HDR-CX405 camcorder from Sony.

The envelope density of the samples was calculated by dividing the sample mass, measured with an ABJ-NM/ABS-N analytical balance from KERN, through the sample volume. This was calculated in the case of monolithic samples with the sample dimensions measured using a Precise PS 7215 caliper



from Burg Wächter. In the case of pellet-shaped samples, the volume was estimated by filling all into a graded cylinder ten times and averaging the result.

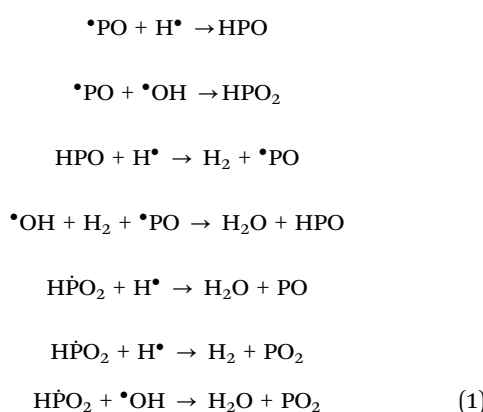
Fourier-transformed infrared (FTIR) analysis were performed with a Spectrum 400 infrared spectrometer equipped with an attenuated total reflection (ATR) crystal, both from PerkinElmer. The measurements were done at room temperature on a cut sample to measure the inner part in the range of 500 to 3500 cm^{-1} with a resolution of 1 cm^{-1} . The presented data are an average of 4 \times 10 scans.

Thermogravimetric analyses (TGA) were performed using a TG 209 F1 Iris thermo-microbalance from NETZSCH. All experiments were performed under the same conditions with a constant nitrogen gas flow of 40 ml min^{-1} , a temperature gradient of 10 K min^{-1} and a temperature range from 25 up to 1000 $^{\circ}\text{C}$.

Results and discussion

Flame-retardant integration and sample densities

The flame-retardant used in this work is the well-investigated triphenyl phosphate (TPP). The burn mechanism, with the key steps depicted in eqn (1), is similar to other organophosphates:



During a fire, the retardants release different organophosphate radicals. These react and recombine with hydrogen and hydroxyl radical to less harmful or unreactive compounds, suffocating the flame.³⁵ For TPP specifically, in addition to

product like carbon (di-)oxides and different phosphorous oxides, the phenyl groups could break off, leading to toxic compound and radicals like benzene and other aromatics during incomplete combustion. At the same time, a variety of aromatic phosphates are also be possible.³⁶

TPP was added by soaking the dried aerogel with a solution of varying concentration (5 to 150 g l^{-1} , see Fig. 1), and then evaporating the solvent at different temperatures (room temperature to 80 $^{\circ}\text{C}$). The change in density of the dried samples can be seen in Table 1.

The experiments with the standard system revealed that evaporation at room temperature is only viable at lower concentrations (up to 25 g l^{-1}) due to otherwise massive increase in density, making them unsuitable for the target application. This range (5 to 25 g l^{-1}) was further investigated at room temperature for the other two systems (diluted monoliths and pellets), while higher (30 to 150 g l^{-1}) were performed at 40, 60 or 80 $^{\circ}\text{C}$. Both room temperature and 40 $^{\circ}\text{C}$ were deemed viable for all three systems. For the diluted samples, 80 $^{\circ}\text{C}$ gave reproducible results, likely due to the overall lower density while maintaining the same dimensions as the standard. Previous research has shown that for these samples, the porosity increased while the particle size decreased compared to the standard,³⁷ leaving more space available for the TPP solution to infiltrate. Additionally, a homogenous evaporation and distribution might require a faster reaction (= higher temperature), because a lower one might lead to more diffusion towards the edges before it vaporizes. In the case of the pellets, the network is identical to the standard as both are products of the same synthesis, but the dimensions are smaller (see Fig. 5). This results in a temperature of 60 $^{\circ}\text{C}$ being enough to evaporate the solution homogenously, because of the smaller distance to the edges leading to faster heat distribution. Other combinations of systems, TPP content or evaporation temperature led to less reproducible densities and were not further investigated.

In order to be a feasible material for lightweight transportation, low density plays a crucial role as higher mass means increased operation costs. Aerogels are generally low-weight and highly porous, leading to densities of the flexible silica monoliths (see Table 1) in the range of 0.115 g cm^{-3} for the



Fig. 1 Growth of TPP excess crystals during evaporation at r.t., with increasing concentration from left to right. These were removed before doing any calculations or experiments.



Table 1 Density of aerogels after storage in TPP/EtOH-solution of different concentrations and varying evaporation temperatures

Concentration [g l ⁻¹]	5	10	15	20	25	30	60	90	120	150
Standard monolith (0.115 g cm ⁻³ untreated)										
Evaporation at r.t.	0.112	0.108	0.111	0.108	0.108	0.133	0.149	0.146	0.153	0.152
Evaporation at 40 °C	—	—	—	—	—	0.111	0.110	0.113	0.125	0.117
Diluted monolith (0.095 g cm ⁻³ untreated)										
Density ^a [g cm ⁻³]	0.094	0.091	0.089	0.090	0.092	—	—	—	—	—
Evaporation at r.t.	—	—	—	—	—	0.092	0.088	0.097	0.110	0.127
Evaporation at 40 °C	—	—	—	—	—	0.094	0.106	0.100	0.112	0.138
Pellets (0.072 g cm ⁻³ untreated)										
Density ^a [g cm ⁻³]	0.088	0.102	0.103	0.159	0.116	—	—	—	—	—
Evaporation at r.t.	—	—	—	—	—	0.093	0.123	0.153	0.186	0.207
Evaporation at 40 °C	—	—	—	—	—	0.098	0.124	0.168	0.183	0.244
Evaporation at 60 °C	—	—	—	—	—	—	—	—	—	—

^a Average of min. two samples, with an error ranging from ±0.004–0.012 g cm⁻³; formatting: italics = no, bold italics = weak and bold = strong TPP-IR-Signals inside of the aerogels, see Fig. 2.

patented standard³⁴ to 0.095 g cm⁻³ for a diluted recipe. This could be further decreased to around 0.072 g cm⁻³ by changing from monoliths to pellets, which intrinsically have additional air-pockets in-between them, reducing the envelope density. While these values are higher than most classic silica aerogels,³⁸ which can range around 0.001 to 0.200 g cm⁻³, hybrid-silica aerogels are hydrophobic and can be dried in ambient conditions, skipping or limiting time consuming and expensive steps like post-hydrophobization, solvent exchange and supercritical drying equipment.

The density of the TPP treated standard system at lower concentration (5 to 25 g l⁻¹) remained similar to the reference, while higher ones (30 to 150 g l⁻¹) at room temperature led to massive increase up to 0.153 g cm⁻³. However, a plateau was already visible starting from 60 g l⁻¹, anything above seems to not add more into the pores. When evaporating at 40 °C, only slight increases within the error margin of the reference were observed, meaning only a small amount was integrated. For the diluted monoliths, at room temperature samples showed similar results to the reference and standard with only a small

increase in density. At 40 °C, a gradual increase towards higher concentration could be seen without plateauing, meaning more loading than the standard could be possible. This is explained by the increased porosity, leaving more space for the flame-retardant. At 80 °C, the density also increased with concentration of TPP, but overall higher than in the 40 °C experiments. The pellets behaved differently: room temperature evaporation already resulted in a big increase in density, while samples both at 40 and 60 °C had a linear increase resulting in even higher values, with 60 °C more pronounced.

Generally, the density of the treated material increased expectedly, with any variation compared to the untreated samples lying within the error margin. As high TPP concentration led to loosely attached crystallites, which were considered overgrowth and thus removed manually, no pore-filling percentage or similar were calculated. More crystals were visible at higher concentrations (= more excess TPP) and lower evaporation temperature, further supporting that the solution diffuses towards the edges before evaporating. This, however, could be mitigated with increased temperatures. In order to

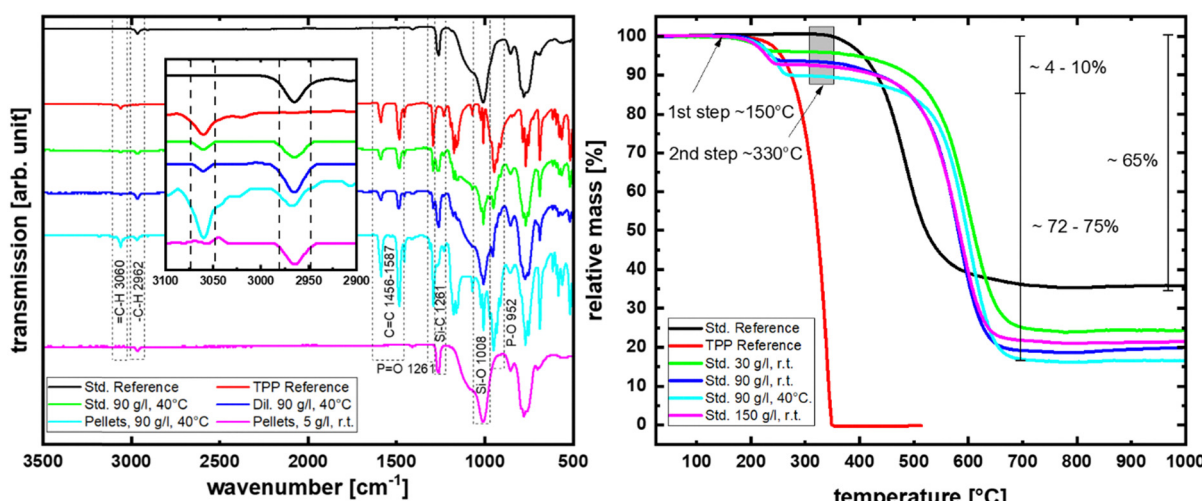
Fig. 2 Stacked IR-spectra (l.) and TGA data (r., under N₂) of selected TPP-treated aerogel samples.

Table 2 IR signals corresponding to the silica network and flame-retardant

Hybrid-silica network	~2960 cm ⁻¹ -C-H stretching	~1260 cm ⁻¹ -C-H bending	~1008 cm ⁻¹ Si-O-Si stretching	—
Flame-retardant TPP	~3060 cm ⁻¹ =C-H stretching	~1450-1590 cm ⁻¹ C=C stretching	~1260 cm ⁻¹ P=O stretching	~950 cm ⁻¹ P-O stretching

verify the integration inside the pores and not only on the edges as surface coating, IR-measurements of cut samples were performed, with the addition of TGA-analysis (see Fig. 2).

The insides of the samples were measured by IR-spectroscopy (see Fig. 2). The hybrid-silica aerogel signals and the TPP signals (see Table 2) correspond to literature values^{39,40} and were present in the corresponding samples, with the exception of the TPP signal at very low concentrations. This verified the integration of TPP inside of the aerogels with the standard parameters for all systems (concentration of 90 g l⁻¹ and evaporation temperature of 40 °C).

TGA measurements also confirmed the integration of the flame-retardant, as an additional step starting around 150 °C could be observed in the treated samples, corresponding to the TPP reference. The mass loss was around 4 to 10% and depended on the amount TPP integrated, which itself relied on the concentration and evaporation temperature of the synthesis. It again seemed that the latter parameter was more significant when comparing the mass loss of room temperature dried samples (~4 to 7%) to 40 °C (~10%). The organic part of the aerogel network started to decompose around 330 °C, similar to observations in literature.⁴¹ As the analysis was performed under nitrogen, this final composition would be some type of silica oxycarbide.⁶

Burn behavior

With the integration of the flame retardant verified, the effect during burn experiments was investigated next. First, the

samples were exposed to a Bunsenburner flame for 20 seconds (40 in the case of no reaction). Afterwards, the progression of the burning was analyzed by logging the different burn stages and their durations (see Fig. 3).

The whole burn process was separated into different stages (see Fig. 3 right): the ignition of the sample (yellow); visible flame (red); orange ember inside the sample (orange); smoke with no flame or ember visible (grey) and sample deformation with no flame, ember or smoke visible (white). These can be seen more clearly in burn progression images (see Fig. 4), showing the standard reference and three different types of TPP treated samples in more detail.

Looking at the references, both untreated monolithic samples completely burn through once ignited, due to no barrier stopping the flame from reaching all organic parts of the network. Pellet samples were inherently more protected, as during the ignition only a few were directly exposed to the flame, shielding the others similar to a sacrificial layer. The reproducibility of the synthesis and treatment was verified by looking at the repeated experiments with identical composition, but from different batches (see Fig. 3 bottom). Here, the burn durations were within 30 seconds for roughly 300 seconds of total duration and the burn stages vary only slightly, with the less severe ones clearly dominating.

All treated samples suppressed an open flame, instead visible white smoke was dominant throughout, an effect of

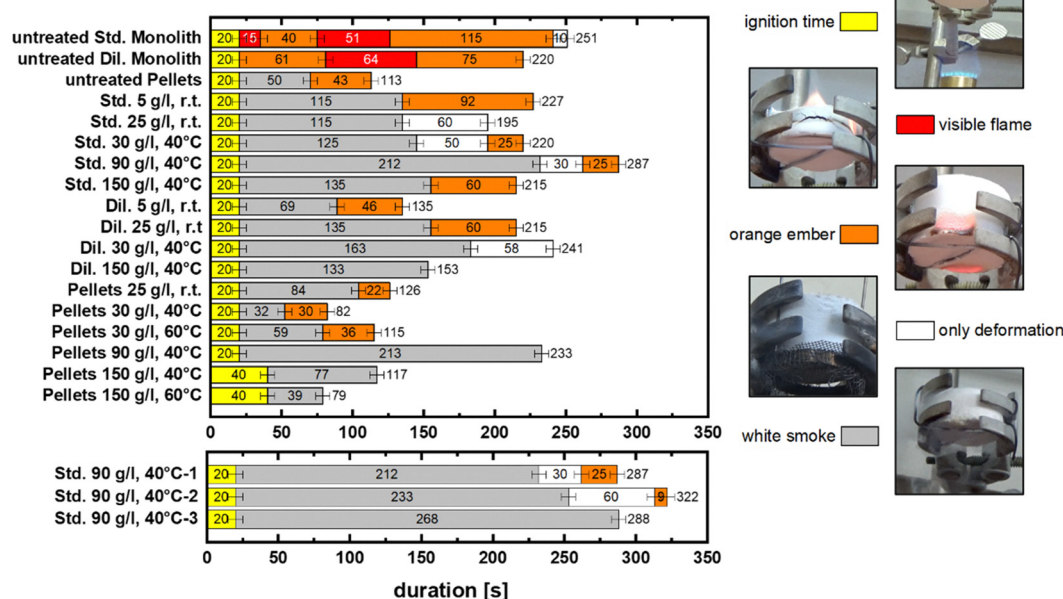


Fig. 3 Burn durations (top l.) and stages (r.) of untreated and selected TPP-treated aerogel samples and the reproducibility of the experiment (bottom l.).



the flame-retardant working as intended. When a lower concentration was used ($<30\text{ g l}^{-1}$), orange embers were still visible, and only in case of the standard monolith they still appear even at higher amount of integrated TPP. This could be a result of the denser network compared to the diluted samples, or small variations in the sample as seen in the reproducibility experiment (see Fig. 3 bottom). For very high concentrations with the inherently better performing pellets, no reaction was observable after 20 seconds of ignition, which is why it was doubled to 40 seconds, yet the reaction still ended very fast.

In general, the duration of the burning process does not correlate clearly to the amount of flame retardant added. A reason could be that, at very low concentration of TPP, the burning process is barely hindered and similar to the references. At very high concentration the burn process is suppressed to a high degree, leading to a faster end of the reaction. This trend was observed in both the diluted monoliths and pellet samples, with standard monoliths not varying much in their duration at all. It is important to note that only a part of the sample could be observed during the experiment, which could lead to slight variations. However, this does not mitigate the general trend observed. The values gained from these experiments were used to rank the different samples in a later

section (see Table 4), which allowed better comparison and discussion.

The burn experiments of selected samples were observed in more details to improve the understanding of the burn progression (see Fig. 4). In case of the untreated standard, the fire after ignition burned through the organic parts of the sample, sometimes breaking out as an open flame. During this, the sample cracked, allowing to observe the burning of the samples inside more clearly. In the end, the sample lost all flexibility and broke with the slightest touch. For the treated standard monolith, the open flame was suppressed and instead white smoke became dominant. Similar to the untreated reference, the sample cracked during this process, but to a much lower degree. While the sample also became stiff, it did not break as easily, an effect of limiting the damage. The diluted monolith behaved similarly with an increased stiffness, but showed no signs of cracking, which could be a further indicator that the lower system density is advantageous. For the pellets, most of them were not affected by the flame at all and remained flexible. Those exposed to the flame did not crack but became slightly stiffer. A detailed look on more samples after burning was also performed (see Fig. 5).

The side exposed to the flame was expectedly charred, and in case of the standard monoliths cracked in most cases, with

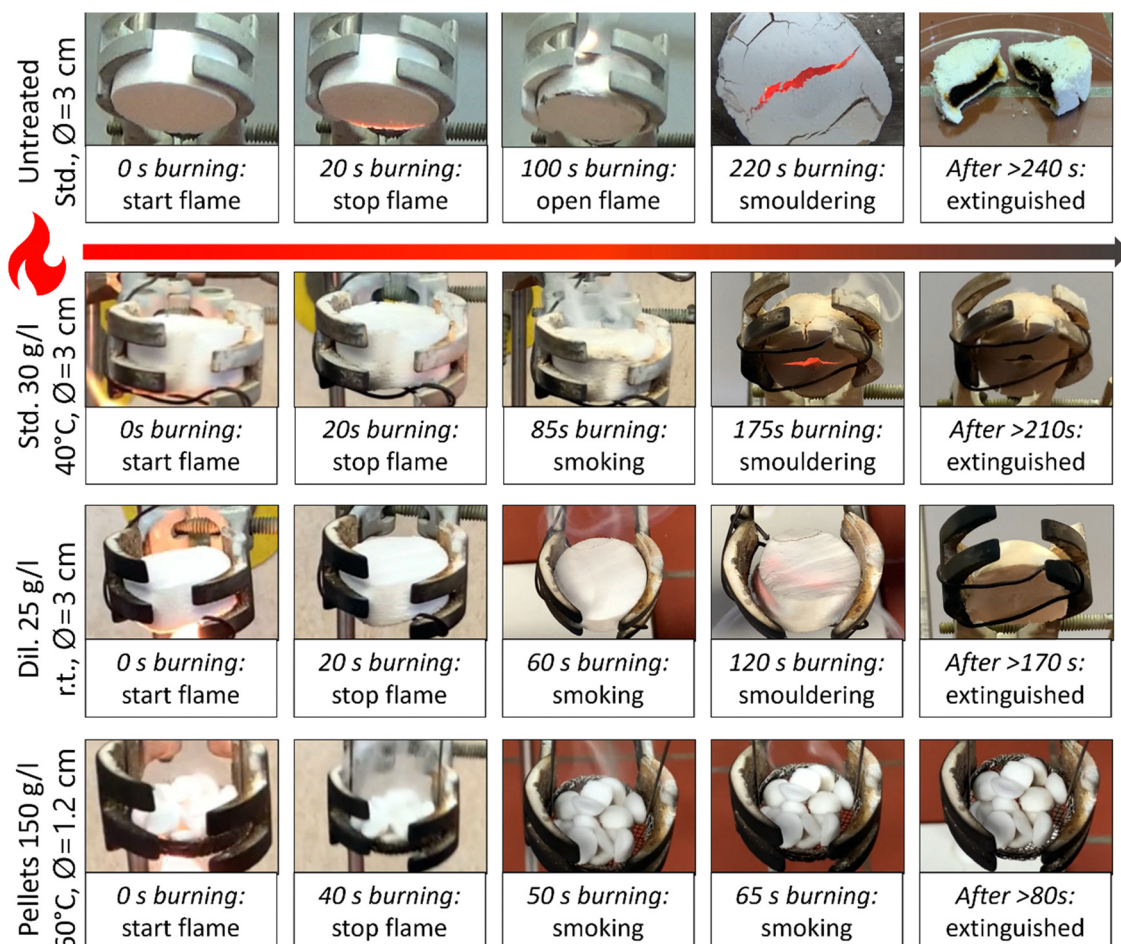


Fig. 4 Detailed progression of selected burn experiments at different times.





Fig. 5 Sample pictures after the burn experiments: side exposed to the flame (top l.); backside (top r.); cross section (bottom l.); pellets (bottom r.).

more damage at lower amount flame-retardant. These cracks propagated to the backside, which was mostly unaffected by the charring, with no clear trend. All monoliths were charred on the inside, as could be seen from the burning of the samples (see Fig. 4). These effects were less grave in the diluted samples, and also further decreases with higher TPP content. For pellets, only those exposed directly to the flame showed a brown discoloration, with most others not visibly affected, meaning the flame did not propagate from one pellet to the next, important information for the use-case. Even less influence of the experiment on the samples can be seen at very high amount of flame-retardant. Changes in morphology were similar: high damage is visible at no/low TPP concentration, as the particles turn from big and round micrometer-sizes to broken nanometer-sizes. But with enough flame-retardant, the effect is very limited, as the TPP forms a visible protective coating (see Fig. S4).

Behavior under simulated conditions

The requirements of an air cabin insulation are different from the lab environment, especially when looking at the operation temperature ranges it will be exposed to. For example in a hot desert airport the ambient temperature can already be very high, with the hull potentially reaching the melting point of the investigated TPP

(49–50 °C).⁴² If this kind of environment could melt the flame-retardant and reduce the burn protection, the material would not be viable. To investigate this, a simulated hot environment to observe the behavior of the samples was prepared (see Fig. 6 top left).

This investigation consisted of several steps: First, several standard monoliths were prepared with the standard conditions (90 g l^{-1} and 40°C), with which the melting experiment (see Fig. 6 top left) and the corresponding mass analysis (see Fig. 6 top right) was performed. The temperature of the plate was set to 100°C , simulating extreme hull temperature, and remained stable over the six-hour duration. This duration was chosen as the expected turn-around of airplanes during the day, where the high temperature is expected, will most likely be lower. During the experiment, both the inside and the surface of one sample each was measured. Looking at the temperature data (see Fig. 6 top left), these reached their stable temperature at around 20 minutes with roughly 40°C and 35°C , respectively, and remained over the 6-hour experiment.

The second part was measuring the masses before and after TPP treatment and after the experiment itself (see Fig. 6 top right) to see if and how much flame-retardant was lost throughout the duration. The reference shows no change, which corresponds to the TG-data where the first decomposition of untreated samples occurred at $\sim 330^\circ\text{C}$ (see Fig. 2). For each

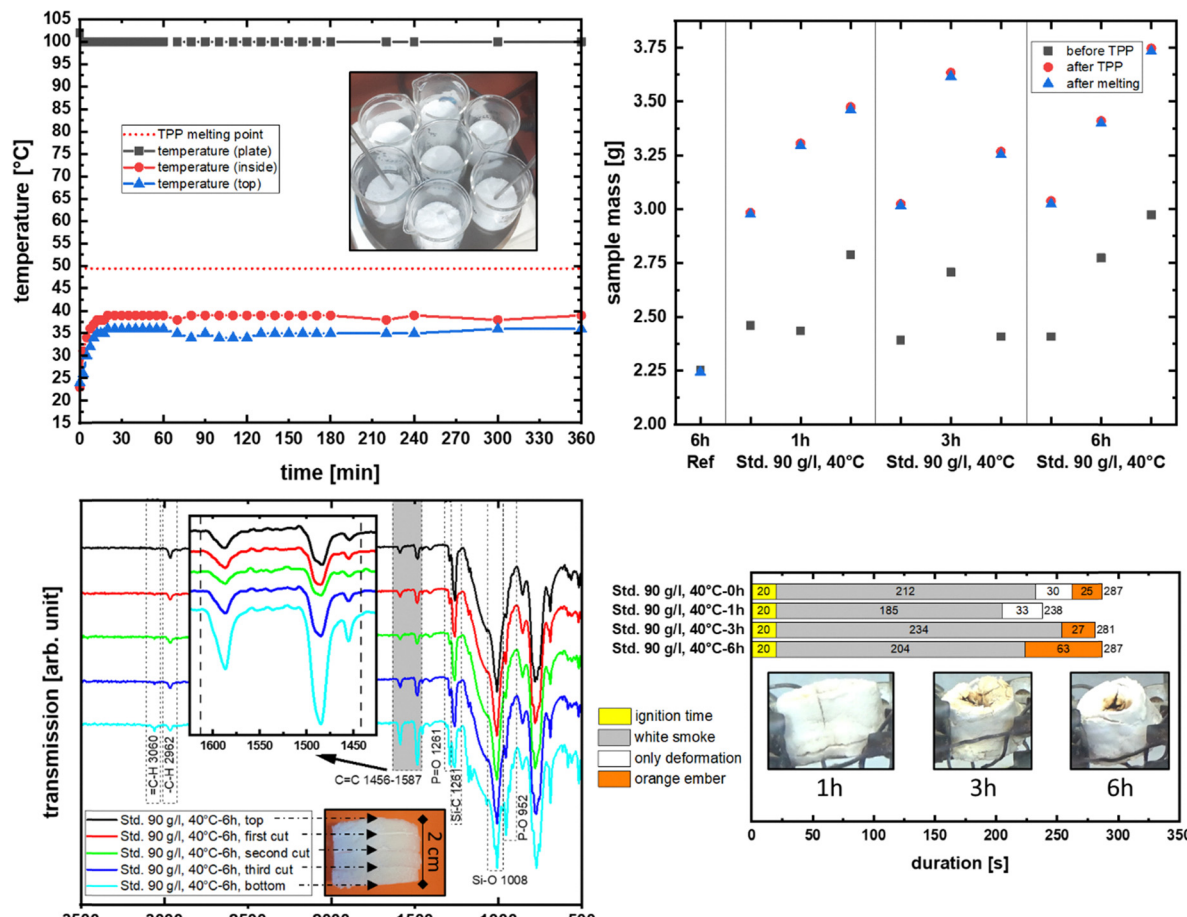


Fig. 6 Melting experiments and analysis of TPP-treated aerogels: temperature development during the experiment (top L); sample masses before/after TPP impregnation and after melting (top R); stacked IR-spectra of sliced samples after melting (bottom L); burn behavior after melting (bottom R).

duration (1, 3 and 6 h), three samples were investigated for statistical reasons. The mass before integration varied due to the experimental setup of the synthesis, and the mass of TPP integrated ranges from ~ 0.5 g to 0.8 g, which was below half of the estimated theoretical maximum of 1.8 g (20 ml of 90 g l⁻¹ TPP solution). In all cases, the mass only decreased very insignificantly after the simulated conditions, meaning a decrease in flame-retardancy could not be a result from the loss of TPP.

While there was no mass loss, it was important to investigate if the TPP melted in the lower half of the sample, producing a rich cover on the bottom and a deficient layer just above it. Depending on the severity of this, it could negatively influence the effect of the flame-retardant, because a protection coating could be breached. For this, IR analysis of a six-hour treated sample cut in several horizontal slices was performed (see Fig. 6 bottom left). Expectedly, some of the TPP on the bottom melted under the experimental conditions of 100 °C and re-solidified, as seen clearly with the intensity C=C double bond vibrations in the region of 1456–1587 cm⁻¹. However, no signs of any deeper depletion could be observed, as all other slices show similar intensity-ratio from the silica-network to the flame retardant.

To further investigate if the samples burn behavior changed, which would indicate a significant change in the homogenous

distribution of the flame retardant, the samples were also used for the burning experiments (see Fig. 6 bottom right). It is clear that they did not behave any different from the reference sample or the other samples used for the reproducibility showcase (see Fig. 3 bottom). This means even under extreme temperature conditions, the flame-retardant effect remains, making them viable for further investigation towards use in airplane insulation.

While long-term or cyclic experiments have not been performed, which would resemble multiple takeoffs or landing, it is expected to lead to further enrichment of TPP on the bottom layer. This in turn would decrease the TPP in the area directly above, leading to properties more closely resembling the untreated aerogel material. This layer would act as a thermal barrier, preventing the higher temperatures from reaching deeper into the material, leading to minimal effect on the bulk of the material. However, this still needs to be experimentally confirmed in future work.

Flame-retardant performance

The acquired data (see Fig. 3) has been used with the following equation to evaluate the flammability of the samples:

$$Fl = \sum \frac{t_{\text{stage}} \cdot S_{\text{stage}}}{100}, \quad (2)$$



Table 3 Different burn stages and their severity factor

Burn stage	Severity S (s^{-1})
Ignition	0
Only deformation	1
White smoke	1.5
Orange ember	3
Visible flame	5

with Fl : flammability; t_{stage} [s]: duration of a certain burn stage and S_{stage} [s^{-1}]: severity of a certain burn-stage (see Table 3). If several stages occur simultaneously, the more severe one was used for the calculation.

The severity was based on the following assumptions:

- The ignition as necessary part of the experiment was left out ($S = 0$).
- Only deformation of the material has negligible severity ($S = 1$), as this is preferable to all the other stages.

– The smoke is considered not ideal, especially in airplanes ($S = 1.5$), but could potentially be filtered through the airduct-system. However, the components of the gas phase and their toxicity has not been investigated, and might lead to an increased severity factor.

– Orange glow inside the sample is considered severe ($S = 3$), as this means an active burning inside the material. It is however still contained.

– An open flame is considered very severe ($S = 5$) due to how easily it could propagate to other materials and the surrounding.

With eqn (2) and the data (see Fig. 3), the samples were ranked on their flame-retardant quality (see Table 4), with low Fl values meaning superior flame protection.

In their respective categories, the untreated samples showed worse behavior compared to the treated samples, which was to be expected. With the exception of the standard monolith system, higher flame-retardant concentration also led to a better flame retardancy, both in their categories and overall. However, this value does not include other important factors, that's why it was used as base for calculations also considering density, and arguably more important parameter for the application, leading to the calculation of the overall sample performance and more detailed discussion (see Table 5).

Looking at literature, not much has been investigated with the same type of MTMS and DMDMS-based flexible hybrid-silica aerogels and flame retardants. For example, inorganic $Mg(OH)_2$ -surface coating⁴³ led to improved flame-retardancy, with a ~19.5% lower average burn-rate. Compared to this, the best sample from this works TPP treatment reached around ~30% lower burn duration (pellets 150 g l^{-1} , 60 °C). As other properties like the density of the $Mg(OH)_2$ -treated samples were not investigated and only one concentration of flame-retardant material was synthesized, a more detailed comparison makes little sense. However, due to the addition of $Mg(OH)_2$ with its high density, the weight and thus density of the treated aerogel is expected to increase more drastically compared to the TPP-coated samples investigated in this work.

Table 4 Ranking based on flame-retardancy of the samples, either by type or in total

Sample	Fl	Rank (by system)	Rank (total)
Untreated std. monolith	8.05	6	18
Std. 5 g l^{-1} , r.t.	4.49	5	16
Std. 25 g l^{-1} , r.t.	2.33	1	8
Std. 30 g l^{-1} , 40 °C	3.13	2	11
Std. 90 g l^{-1} , 40 °C	4.23	4	15
Std. 150 g l^{-1} , 40 °C	3.83	3	13
Untreated dil. monolith	7.28	5	17
Dil. 5 g l^{-1} , r.t.	2.42	2	9
Dil. 25 g l^{-1} , r.t.	3.83	4	13
Dil. 30 g l^{-1} , 40 °C	3.03	3	10
Dil. 150 g l^{-1} , 40 °C	2.00	1	6
Untreated pellets	2.04	6	7
Pellets 25 g l^{-1} , r.t.	1.92	4	4
Pellets 30 g l^{-1} , 40 °C	1.38	3	3
Pellets 30 g l^{-1} , 60 °C	1.97	5	5
Pellets 90 g l^{-1} , 40 °C	3.20	7	12
Pellets 150 g l^{-1} , 40 °C	1.16	2	2
Pellets 150 g l^{-1} , 60 °C	0.59	1	1

Another comparison can be made looking at this works physical coating to chemically bonded organophosphates, for example vinylphosphonic acid (VPA).⁴⁴ It has been shown that all VPA-treated materials decrease drastically in temperature when flame is removed, with no further burning visible. The end of their reaction was reached after around 200–250 s with VPA-treatment, compared to around 500 s without. This reduction of 40 to 50% is even higher than with TPP-treatment. The density increased by around 10% for VPA-samples, compared to 5 to 30% of TPP samples, depending on the loading concentrations. Overall, the chemical bond allows better homogenous distribution throughout the material, which is challenging to achieve with physical methods. TPP-treatment will always add additional mass and increase the density of the aerogels. However, it can be done much easier and for a broad range of materials, unlike the complex fabricate of VPA-treated samples.

Table 5 Ranking based on overall quality of the samples, either by type or in total

Sample	Fl	Density ($g cm^{-3}$)	Quality Q	Rank (by system)	Rank (total)
Untreated std. monolith	8.05	0.115	3.19	6	18
Std. 5 g l^{-1} , r.t.	4.49	0.112	5.95	5	15
Std. 25 g l^{-1} , r.t.	2.33	0.108	12.12	1	7
Std. 30 g l^{-1} , 40 °C	3.13	0.111	8.65	2	12
Std. 90 g l^{-1} , 40 °C	4.23	0.113	6.22	4	14
Std. 150 g l^{-1} , 40 °C	3.83	0.117	6.53	3	13
Untreated dil. monolith	7.28	0.095	4.69	5	17
Dil. 5 g l^{-1} , r.t.	2.42	0.094	14.37	1	4
Dil. 25 g l^{-1} , r.t.	3.83	0.092	9.37	4	10
Dil. 30 g l^{-1} , 40 °C	3.03	0.092	11.85	2	8
Dil. 150 g l^{-1} , 40 °C	2.00	0.127	11.08	3	9
Untreated pellets	2.04	0.072	25.37	2	2
Pellets 25 g l^{-1} , r.t.	1.92	0.116	13.18	5	6
Pellets 30 g l^{-1} , 40 °C	1.38	0.093	25.55	1	1
Pellets 30 g l^{-1} , 60 °C	1.97	0.098	16.59	3	3
Pellets 90 g l^{-1} , 40 °C	3.20	0.153	5.23	7	16
Pellets 150 g l^{-1} , 40 °C	1.16	0.207	9.19	6	11
Pellets 150 g l^{-1} , 60 °C	0.59	0.244	14.18	4	5



Overall sample performance for lightweight application

In order to include important properties like the density in the ranking, eqn (3) was used for further calculations:

$$Q = \frac{1}{\rho^{1.5} \cdot \text{Fl}} \cdot C, \quad (3)$$

with Q : overall quality of the sample; ρ : density of the sample [g cm^{-3}]; Fl : flammability (see eqn (2)) and C : a constant with the value 1 [$(\text{g cm}^{-3})^{1.5}$].

It is based on the premise that lower density is more important than pure flame-retardant effect, specifically for the use-case in airplanes where more weight results in massively increased operation costs. Additionally, while the thermal conductivity plays an important role for these aerogels and their overall performance as material, previous studies have shown that the systems investigated here show minimal difference.³⁷

Compared to only looking at the flammability, the ranking by quality gives a more general idea which samples could be feasible as insulation material for air cabins.

In both monolithic systems, the references remained unexpectedly worse than any treated samples. For this type, a medium concentration of TPP (25 or 30 g l^{-1}) gave the best results, afterwards higher concentration showed more promise than lower. This is due to the overall density not increasing by much, even with high amount of flame retardant added, which would just lead to more excess crystals which were removed (see Fig. 1). Overall, the standard system remained the worst of those investigated.

The comparison for the diluted system led to the opposite conclusion for this type: Very low (5 g l^{-1}) amount of flame-retardant led to the best results, with medium amount (30 g l^{-1}) and very high amount (150 g l^{-1}) being very similar. The first trumps with low density, albeit only adequate flame-retardancy, while the latter exhibits excellent burn-protection, but at the cost of much higher density. Overall, these samples are superior to the standard monoliths, but worse than the pellet system. The exception was the one with lowest concentration, which ranked fourth compared to all others.

For the pellet system, the untreated takes the second spot in both its category and the total ranking, only beaten by another pellet sample treated with a medium amount of flame retardant (30 g l^{-1}). This is because this type itself showed already good flame-retarding properties by sacrificing a few pellets, while protecting the others. Those produced with a higher concentration had a massive increase in density, leading to an overall worse ranking. The overall performance however was above the other two systems. This again exemplifies the impact on the sample system, with untreated pellets being inherently better.

Conclusions

Three different hybrid-silica aerogel systems were investigated towards changes of their properties through the addition of TPP as flame-retardant. The density values revealed that the untreated references from standard to diluted to pellet systems

decreased, while higher TPP infusion led to an expected increase. It could be pinpointed that the evaporation of the flame-retardant solution at room temperature was only viable for low concentration, and the effect on the density was either negligible (in case of monoliths) or already too massive for use in lightweight applications (pellets). For higher concentration, temperatures of 40 to 80 °C resulted in homogenous distribution and reproducible densities. The integration throughout the samples was verified by IR, and even remained after exposure to high operating temperature (~100 °C) for several hours, with no negative effect on the flame-retardancy.

To see the efficiency of the TPP-treatment, the samples were exposed to fire. The untreated monoliths burned with an open flame due to their many unprotected organic parts, which could be prevented with the addition of TPP. To analyze the burning-behavior, these experiments were evaluated into different stages with corresponding severity, with the results used to calculate the flammability and overall quality of the sample for the target application in lightweight transportation. Here, the inherently better pellets ranked top, with diluted monolith above the standard system. The samples were also affected during the burning: The standard aerogels often cracked and became brittle, while the diluted were stiff afterwards but with fewer cracks. For pellets, only a few were damaged by the flame and stiffened, while the others not exposed to the flame showed no change at all, meaning the flame did not propagate from one pellet to the next. The extend of all these generally decreased with increased TPP content.

By calculating a quality value for the samples, which gave a higher significance to the density than the flame-retarding performance due to its importance in the application, all samples could be compared and ranked in their own category and overall. For both monolith systems, standard was usually worse than the diluted system. The former showed better performance at medium loading of TPP, while the other showed superior quality at very low concentrations. The pellets performed better in general, even more at medium loading. However, while it is relatively simple to scale the monoliths to different sizes and use them *e.g.* as mats, the pellets are a completely different system needing additional packaging and installation procedure. Additionally, the abrasion of each other through vibration, which might happen during flight, needs to be investigated to truly estimate the pellets' viability.

Overall, with the developed infusion recipe, the best range of flame-retardant loading with minimal negative influence on the density was found out for the different hybrid-silica aerogel systems. Based on this, further development towards the application as lightweight insulation material can be conducted, especially looking at scaling and other important properties like acoustic performance.

Authorship contribution

Danny Bialusiewski: conceptualization, investigation, methodology, validation, data curation, formal analysis, writing – original



draft, writing – review & editing. Kai Steffens: Conceptualization, Investigation, Methodology, validation. Prof. Barbara Milow: supervision, funding acquisition, project administration.

Conflicts of interest

There are no conflicts to declare.

Data availability

All relevant data is part of this publication. The SI shows the remaining IR-Spectra not presented in Fig. 2 (Fig. S11–3, standard, diluted and Pellet samples respectively) and SEM images for the morphological comparison before and after burning. See DOI: <https://doi.org/10.1039/d5ma00695c>. The video files of the burn experiments used is available in the zenodo online repository under <https://doi.org/10.5281/zenodo.1551759>

Acknowledgements

The authors gratefully acknowledge the funding by the Federal Ministry of Economic Affairs and Climate Action (BMWK) and its Aviation Research Program “LuFo VI-1” with “LABKABIN”, part of the joint project “MULTIKABIN” (FKZ: 20Q1908C). The authors also thank the University of Cologne for providing the facilities to perform this research and Dr Thomas Anklam for performing the SEM analysis.

References

- 1 S. S. Kistler, *Nature*, 1931, **127**, 741.
- 2 S. S. Kistler, *J. Phys. Chem.*, 1932, **36**, 52–64.
- 3 N. Bheekhun, A. R. Abu Talib and M. R. Hassan, *Adv. Mater. Sci. Eng.*, 2013, **2013**, 406065.
- 4 M. Schmidt and F. Schwertfeger, *J. Non-Cryst. Solids*, 1998, **225**, 364–368.
- 5 D. Pico, E. Meyer, A. Luking, B. Milow and T. Gries, *Chem. Eng. Trans.*, 2017, **60**, 91–96.
- 6 T. Welsch, Y. Vievers, M. Schnellenbach-Held, D. Bialuszewski and B. Milow, *Gels*, 2023, **9**, 406.
- 7 G. Hayase, K. Kanamori and K. Nakanishi, *J. Mater. Chem.*, 2011, **21**, 17077–17079.
- 8 G. Hayase and Y. Ohya, *Appl. Mater. Today*, 2017, **9**, 560–565.
- 9 C. Sanchez, B. Julián, P. Belleville and M. Popall, *J. Mater. Chem.*, 2005, **15**, 3559–3592.
- 10 G. Zu, K. Kanamori, T. Shimizu, Y. Zhu, A. Maeno, H. Kaji, K. Nakanishi and J. Shen, *Chem. Mater.*, 2018, **30**, 2759–2770.
- 11 G. Zu, T. Shimizu, K. Kanamori, Y. Zhu, A. Maeno, H. Kaji, J. Shen and K. Nakanishi, *ACS Nano*, 2018, **12**, 521–532.
- 12 Y. Shi, B. Yu, X. Wang and A. C. Y. Yuen, *Front. Mater.*, 2021, **8**, 703123.
- 13 A. Rege, P. Voepel, E. Okumus, M. Hillgärtner, M. Itskov and B. Milow, *Materials*, 2019, **12**, 2878.
- 14 A. Y. Zverev, *Acoust. Phys.*, 2016, **62**, 478–482.
- 15 M. Bagshaw and P. Illig, in *Travel Medicine*, ed. J. S. Keystone, P. E. Kozarsky, B. A. Connor, H. D. Nothdurft, M. Mendelson and K. Leder, Elsevier, London, 4th edn, 2019, pp. 429–436, DOI: [10.1016/B978-0-323-54696-6.00047-1](https://doi.org/10.1016/B978-0-323-54696-6.00047-1).
- 16 G. Grün, M. Trimmel and A. Holm, *Build. Environ.*, 2012, **47**, 23–31.
- 17 J. Cox, A. Markey, R. Kohn, N. J. Butcher, M. Moxon, M. Knowles, P. Moxham, K. Abbott, B. Burian, P. Richards, D. Martin, J. Barnett and P. Terry, *International Air Safety Seminar Proceedings*, 2013, 14–79.
- 18 E. Schmitt, *Plast. Addit. Compd.*, 2007, **9**, 26–30.
- 19 B. Schartel, in *Plastics Flammability Handbook*, ed. J. Troitzsch and E. Antonatus, Hanser, 4th edn, 2021, pp. 23–52, DOI: [10.3139/9781569907634.002](https://doi.org/10.3139/9781569907634.002).
- 20 X. Chen, Y. Hu and L. Song, *Polym. Eng. Sci.*, 2008, **48**, 116–123.
- 21 J. Li, H. Zhao, H. Liu, J. Sun, J. Wu, Q. Liu, Y. Zheng and P. Zheng, *RSC Adv.*, 2023, **13**, 22639–22662.
- 22 G. Wypych, in *Handbook of Fillers*, ed. G. Wypych, ChemTec Publishing, 4th edn, 2016, pp. 13–266, DOI: [10.1016/B978-1-895198-91-1.50004-X](https://doi.org/10.1016/B978-1-895198-91-1.50004-X).
- 23 A. K. Greaves and R. J. Letcher, *Bull. Environ. Contam. Toxicol.*, 2017, **98**, 2–7.
- 24 M. Aresta, P. Caramuscio, L. De Stefano and T. Pastore, *Waste Manage.*, 2003, **23**, 315–319.
- 25 I. van der Veen and J. de Boer, *Chemosphere*, 2012, **88**, 1119–1153.
- 26 K. H. Pawlowski and B. Schartel, *Polym. Int.*, 2007, **56**, 1404–1414.
- 27 C. Yao, H. Yang and Y. Li, *Sci. Total Environ.*, 2021, **795**, 148837.
- 28 Z. Zhang, X. Wang, G. Zu, K. Kanamori, K. Nakanishi and J. Shen, *Mater. Des.*, 2019, **183**, 108096.
- 29 W. Jixuan, Z. Chunxia, L. Yunchao, L. Yuntao, S. Zhangmei, X. Dong and L. Hui, *Polym. Eng. Sci.*, 2021, **61**, 693–705.
- 30 K. Opwis, A. Wego, T. Bahners and E. Schollmeyer, *Polym. Degrad. Stab.*, 2011, **96**, 393–395.
- 31 F. Uddin, *J. Ind. Text.*, 2016, **45**, 1128–1169.
- 32 S. Gaan and G. Sun, *Polym. Degrad. Stab.*, 2007, **92**, 968–974.
- 33 S. V. Levchik and E. D. Weil, *J. Fire Sci.*, 2006, **24**, 345–364.
- 34 R. Fener and P. Niemeyer, *Germany Pat.*, EP3042884 B1, 2023.
- 35 B. Schartel, *Materials*, 2010, **3**, 4710–4745.
- 36 D. R. Kirklin and E. S. Domalski, *J. Chem. Thermodyn.*, 1989, **21**, 449–456.
- 37 K. Steffens, D. Bialuszewski and B. Milow, *J. Sol-Gel Sci. Technol.*, 2024, **112**, 768–775.
- 38 S. Zhao, G. Siqueira, S. Drdova, D. Norris, C. Ubert, A. Bonnin, S. Galmarini, M. Ganobjak, Z. Pan, S. Brunner, G. Nyström, J. Wang, M. M. Koebel and W. J. Malfait, *Nature*, 2020, **584**, 387–392.
- 39 R. Al-Oweini and H. El-Rassy, *J. Mol. Struct.*, 2009, **919**, 140–145.
- 40 T. Mahendra Kumar, B. Alice, T. Dahryn, N. Gopal, B. Khemraj and J. Snehasis, *Am. J. Appl. Chem.*, 2015, **3**, 168–173.
- 41 S. Shafi and Y. Zhao, *J. Porous Mater.*, 2020, **27**, 495–502.
- 42 TRIPHENYL PHOSPHATE (ICSC: 1062), Standards of Conduct for the International Civil Service, 2000.
- 43 C. Liu, S. Wu, Z. Yang, H. Sun, Z. Zhu, W. Liang and A. Li, *ACS Omega*, 2020, **5**, 8638–8646.
- 44 K. Steffens, PhD thesis, University of Cologne, 2024.

